

Properties of Secondary Cosmic Ray Nuclei: Eleven-year Results from the Alpha Magnetic Spectrometer

Qi Yan^{a,*} and Vitaly Choutko^a

^aMassachusetts Institute of Technology (MIT), Cambridge, MA 02139, USA

E-mail: qyan@cern.ch, choutko@mit.edu

We report the properties of secondary cosmic rays lithium (Li), beryllium (Be), boron (B), and fluorine (F) measured in the rigidity (momentum per unit charge) range from 2 GV to 3 TV. The measurements are based on 5.1 million lithium, 2.4 million beryllium, 7.1 million boron, and 0.41 million fluorine nuclei collected by the Alpha Magnetic Spectrometer (AMS) on the International Space Station from May 19, 2011 to Nov 11, 2022. The properties of the secondary cosmic ray fluxes and their ratios to the primary cosmic rays Li/C, Be/C, B/C, Li/O, Be/O, B/O, and F/Si, are presented.

38th International Cosmic Ray Conference (ICRC2023)
26 July - 3 August, 2023
Nagoya, Japan



*Speaker

1. Introduction

There are two kinds of cosmic rays. Primary cosmic rays, such as He, C, O, Ne, Mg, Si, S, and Fe, are mainly produced and accelerated at astrophysical sources, while secondary cosmic rays, such as Li, Be, B, and F, are produced by the collisions of heavier nuclei with the interstellar media. Precise knowledge of the rigidity dependence of the secondary cosmic ray fluxes and secondary-to-primary flux ratios is essential in the understanding of cosmic ray propagation in the Galaxy.

The Alpha Magnetic Spectrometer (AMS) is a unique large acceptance, long duration magnetic spectrometer in space, operating aboard the International Space Station at an altitude of 410 km. The primary physics objectives of AMS include measuring energy spectra of cosmic-ray charged particles, nuclei, antiparticles, antinuclei, and gamma-rays to understand Dark Matter, antimatter, and the origin of cosmic rays, as well as to explore new physics phenomena.

In this paper, we report the latest AMS measurements of secondary cosmic ray fluxes of Li, Be, B, and F as well as their ratios to the primary cosmic ray fluxes of Li/C, Be/C, B/C, Li/O, Be/O, B/O, and F/Si, in the rigidity range from 2 GV to 3 TV. These measurements are based on the data collected by AMS during the first 11 years (from May 19, 2011 to Nov 11, 2022) of operation.

2. AMS Detector

The layout of the AMS detector is shown in Fig. 1. The key elements for the measurements in this paper are the permanent magnet, the nine layers, L1-L9, of silicon tracker [1–3] and the four planes of time of flight TOF scintillation counters [4]. Further information on the AMS layout and performance is detailed in Ref. [5].

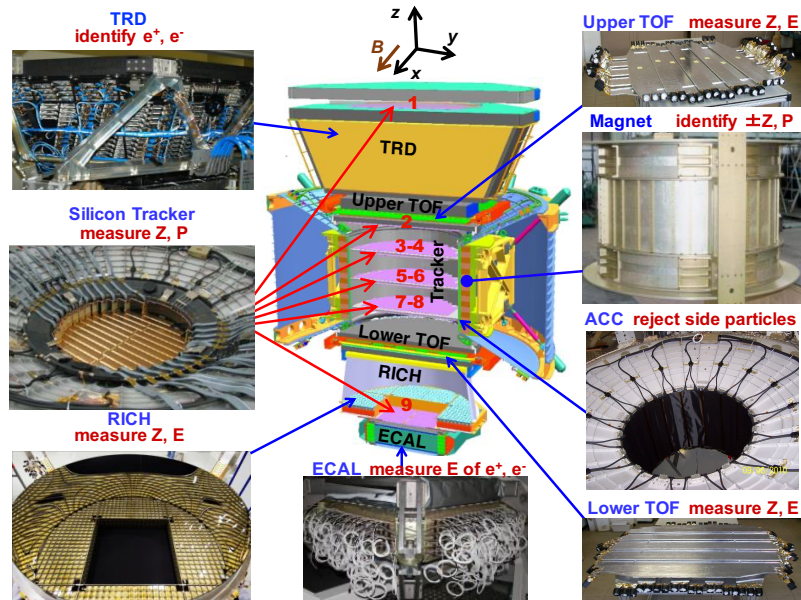


Figure 1: The AMS detector and its main components.

3. Data Analysis

The isotropic flux Φ_i in the i th rigidity bin ($R_i, R_i + \Delta R_i$) is given by

$$\Phi_i = \frac{N_i}{A_i \epsilon_i T_i \Delta R_i}, \quad (1)$$

where N_i is the number of events after background subtraction and correction for bin-to-bin migration due to finite tracker rigidity resolution, A_i is the effective acceptance, ϵ_i is the measured trigger efficiency, T_i is the collection time (which increases with rigidity due to the geomagnetic field, reaching 2.4×10^8 s above 30 GV), and ΔR_i is the rigidity bin width chosen according to the rigidity resolution and available statistics.

The main background for the measurements of secondary cosmic rays in AMS comes from heavier nuclei, which interact above tracker $L2$. It has two sources. First, the background resulting from interactions in the material between $L1$ and $L2$ (TRD and upper TOF) is evaluated by fitting the charge distribution of tracker $L1$ [6, 7]. Second, the background from interactions on materials above $L1$ (thin support structures made by carbon fiber and aluminum honeycomb) has been estimated from simulation using Monte Carlo samples generated according to AMS flux measurements [5]. The simulation of nuclear interactions has been validated with data using nuclear charge changing cross-sections measured by AMS [8]. The uncertainty in each flux (Li, Be, B, and F) due to background subtraction is $< 1.5\%$ at 2 GV, 2% at 100 GV and 2-6% at 3 TV.

The rigidity resolution function for each nuclei element [2] has been studied following the procedure described in Ref. [9]. The resulting systematic error on the flux is $< 1\%$ below 200 GV and smoothly increasing to 7-9% at 3 TV.

There are two contributions to the systematic uncertainty on the rigidity scale. The first is due to residual tracker misalignment. This error was estimated by comparing the E/p ratio for electrons and positrons, where E is the energy measured with the ECAL and p is the momentum measured with the tracker. It was found to be $1/34 \text{ TV}^{-1}$ [1, 10]. The second systematic error on the rigidity scale arises from the magnetic field map measurement and its temperature corrections. The error on the flux due to uncertainty on the rigidity scale is $< 1\%$ up to 200 GV and increases smoothly to 5-7% at 3 TV.

The systematic error on the fluxes associated with the trigger efficiency measurement is $< 1\%$ over the entire rigidity range.

The effective acceptances A_i were calculated using Monte Carlo simulation and corrected for small differences between the data and simulated events related to a) event reconstruction and selection, charge determination, and tracker quality cuts and b) the details of inelastic interactions of nuclei in the AMS materials. The systematic errors on the fluxes associated with the reconstruction and selection are $< 1\%$ over the entire rigidity range. The survival probabilities of Li, Be, B, and F nuclei due to interactions in the materials were evaluated using cosmic ray data collected by AMS as described in Ref. [8]. The systematic error due to uncertainties in the evaluation of the inelastic cross section is $< 3\%$ up to 100 GV. Above 100 GV, the small rigidity dependence of the cross section from the Glauber-Gribov model [11] was treated as an uncertainty and added in quadrature to the uncertainties from the measured interaction probabilities [8]. The corresponding systematic error on each flux is $< 3\%$ up to 100 GV and rises smoothly to 3-4% at 3 TV.

4. Results

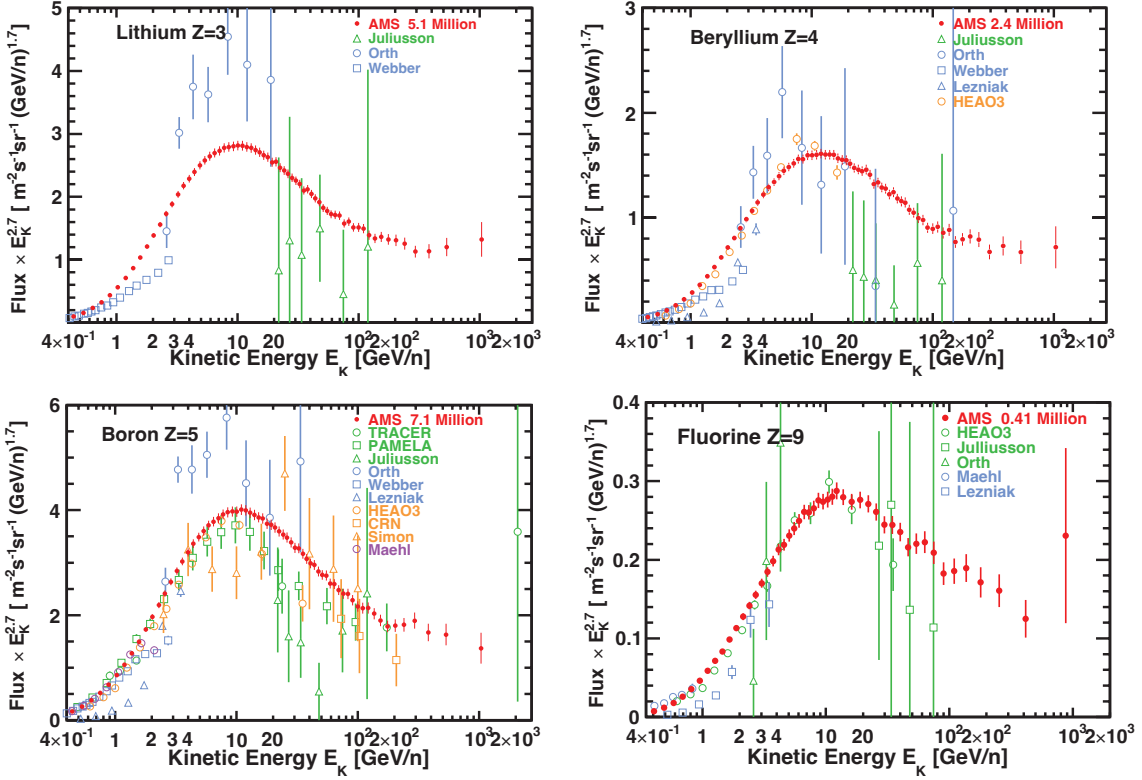


Figure 2: The 11-year AMS fluxes of Li, Be, B, and F as a function of kinetic energy per nucleon E_k multiplied by $E_k^{2.7}$ together with earlier measurements [12–21].

Figure 2 shows the latest AMS fluxes of Li, Be, B, and F as a function of kinetic energy per nucleon E_k together with earlier measurements [12–21]. The AMS measurements are based on 5.1 million lithium, 2.4 million beryllium, 7.1 million boron, and 0.41 million fluorine nuclei collected during the first 11 years of operation.

Li, Be, and B — Figure 3 shows the 11-year AMS fluxes of Li, Be, and B together with the primary cosmic ray fluxes of He, C, and O, as a function of rigidity. As seen, the Li, Be, and B secondary cosmic ray fluxes have identical rigidity dependence above 30 GV. Notably, all three fluxes — Li, Be, and B — deviate from a single power law at high rigidities and harden in an identical way [6]. This behavior is also observed in the primary cosmic rays He, C, and O, but the rigidity dependences of the primary and secondary cosmic rays are distinctly different. To study the difference of the rigidity dependence between the fluxes of Li-Be-B and He-C-O, the Li/C, Be/C, B/C and Li/O, Be/O, B/O flux ratios were fitted above 60 GV with a broken power law function:

$$\begin{cases} k (R/R_0)^{\Delta_1}, & R \leq R_0 \text{ GV}, \\ k (R/R_0)^{\Delta_2}, & R > R_0 \text{ GV}. \end{cases} \quad (2)$$

The fit results with $R_0 = 192$ GV are shown in Fig. 4. As seen, above ~ 200 GV, the spectral indices of Li/C, Be/C and B/C exhibit an average hardening of $\Delta_2 - \Delta_1 = 0.094 \pm 0.023$ and the spectral indices of Li/O, Be/O and B/O exhibit an average hardening of $\Delta_2 - \Delta_1 = 0.133 \pm 0.025$.

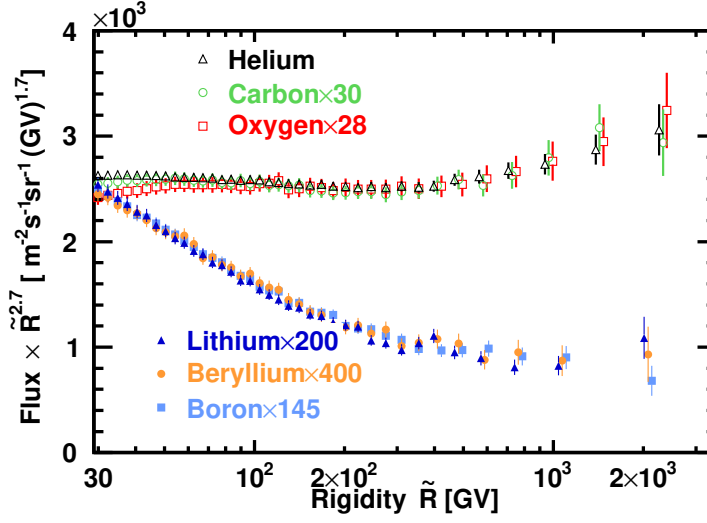


Figure 3: Comparison of the 11-year AMS secondary cosmic ray fluxes of Li, Be, and B with the primary cosmic ray fluxes of He, C, and O multiplied by $\tilde{R}^{2.7}$, together with their total error, as functions of rigidity above 30 GV. As seen, the three secondary fluxes have an identical rigidity dependence above 30 GV, as do the three primary fluxes above 60 GV.

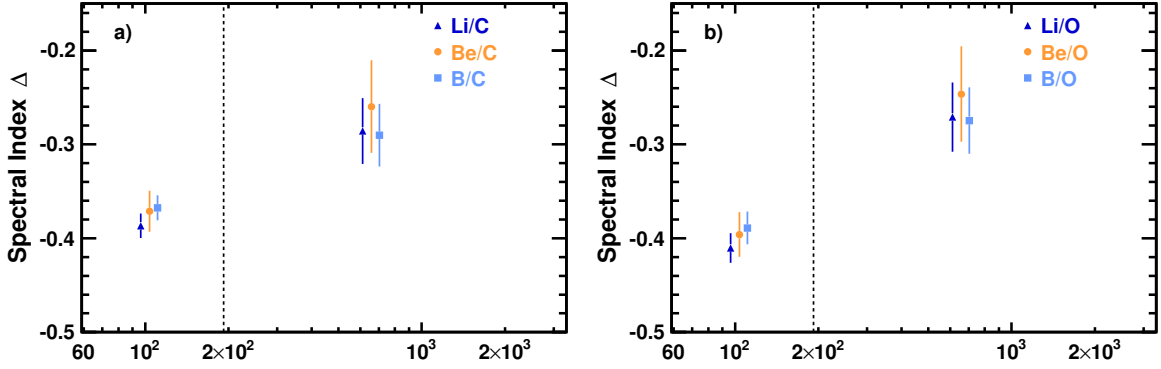


Figure 4: The spectral indices of the 11-year AMS secondary to primary flux ratios (Δ) from Eq. (2) as functions of rigidity for (a) Li/C, Be/C, and B/C and for (b) Li/O, Be/O, and B/O. The vertical dashed line represents the R_0 value of 192 GV. On average, the spectral indices of Li/C, Be/C, B/C, Li/O, Be/O, and B/O exhibit a significant hardening above ~ 200 GV, with a value of $\Delta_2 - \Delta_1 = 0.11 \pm 0.02$ (a 5.5σ significance).

Above 45 GV, we can also fit the flux ratio of characteristic secondary flux B to characteristic primary flux O (B/O) with a double power law function:

$$\Phi = C \left(\frac{R}{45 \text{ GV}} \right)^\gamma \left[1 + \left(\frac{R}{R'_0} \right)^{\Delta\gamma/s} \right]^s \quad (3)$$

The fit yields $\gamma^{B/O} = -0.40 \pm 0.01$, $\Delta\gamma^{B/O} = 0.13 \pm 0.06$, $s = 0.05 \pm 0.04$, and $R'_0 = 200 \pm 88$ GV with $\chi^2/d.o.f = 21/29$. The observed hardening in the B/O ratio, $\Delta\gamma^{B/O} = 0.13 \pm 0.06$, is in good

agreement with the hardening observed in the primary O flux of $\Delta\gamma^O = 0.16 \pm 0.03$, obtained using the same fitting equation. Remarkably, the latest AMS result shows that above ~ 200 GV the secondary cosmic rays harden nearly twice as much as the primary cosmic rays. This favours the hypothesis that the hardening is related to propagation properties in the Galaxy [22–25].

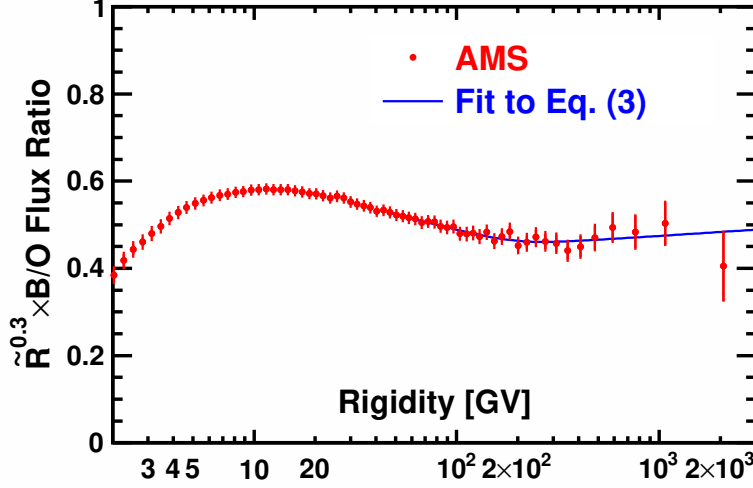


Figure 5: The AMS B/O flux ratio multiplied by $\tilde{R}^{0.3}$ as a function of rigidity R . The solid curve indicates the fit of Eq. (3) to the data.

F — We have previously reported that primary cosmic ray fluxes (with $Z \geq 2$) have two distinct classes of rigidity dependencies above 90 GV: He-C-O-Fe and Ne-Mg-Si-S [26–29]. To study their propagation properties, it is crucial to investigate the secondary cosmic ray fluxes, specifically their ratios to the primary cosmic rays.

Figure 6 left panel shows the 11-year AMS secondary-to-primary F/Si flux ratio together with the B/O flux ratio. To determine the rigidity dependence of the spectral index in the secondary-to-primary ratio, we performed a fit to the F/Si flux ratio using Eq. (2) above 28.8 GV with $R_0 = 175$ GV. The fit yields $\Delta_1^{F/Si} = -0.33 \pm 0.02$ and $\Delta_2^{F/Si} = -0.19 \pm 0.06$, with a $\chi^2/d.o.f.=11/16$. Above 175 GV, the spectral index of the F/Si flux ratio exhibits a hardening of $\Delta_2^{F/Si} - \Delta_1^{F/Si} = 0.14 \pm 0.06$, which is consistent with the AMS result on the B/O flux ratio hardening of $\Delta_2^{B/O} - \Delta_1^{B/O} = 0.12 \pm 0.02$, where $\Delta_1^{B/O} = -0.395 \pm 0.005$, $\Delta_2^{B/O} = -0.28 \pm 0.02$, and $\chi^2/d.o.f.=28/36$.

To conduct a detailed comparison of the rigidity dependence between the F/Si flux ratio and the lighter secondary-to-primary B/O flux ratio, the $\frac{F/Si}{B/O}$ ratio was computed, as shown in Fig. 6 right panel. The $\frac{F/Si}{B/O}$ can also be fitted with Eq. (2) over the entire rigidity range. The fit yields $k = 0.39 \pm 0.01$, $R_0 = 9.8 \pm 0.9$ GV, $\Delta_1 = -0.05 \pm 0.01$, and $\Delta_2 = 0.055 \pm 0.006$, with a $\chi^2/d.o.f.=24/46$. The 11-year AMS result shows that, above 10 GV, the $\frac{F/Si}{B/O}$ ratio can be described by a single power law $\propto R^\delta$ with $\delta(\Delta_2) = 0.055 \pm 0.006$, which exhibits a difference of $> 7\sigma$ from zero. This shows that the heavier secondary-to-primary F/Si flux ratio rigidity dependence is distinctly different from the lighter B/O rigidity dependence, indicating that the propagation properties of heavy cosmic rays, from F to Si, are different from those of light cosmic rays, from

He to O.

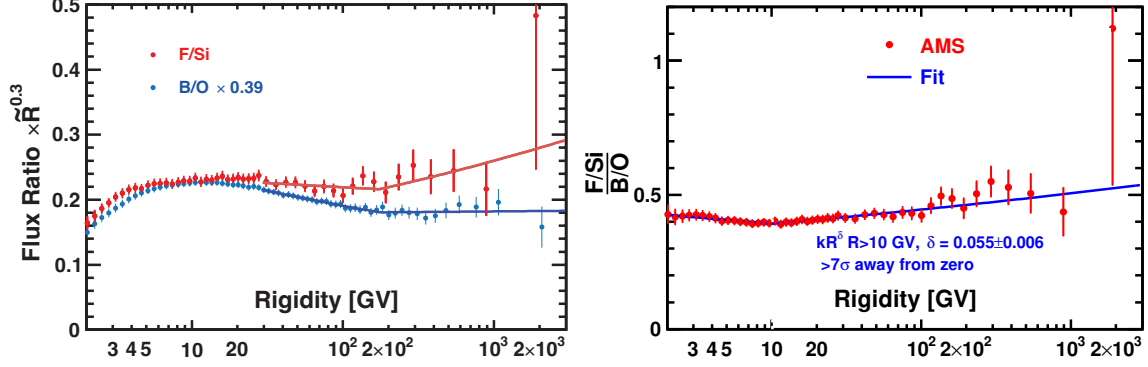


Figure 6: Left panel: The 11-year AMS F/Si flux ratio and B/O flux ratio as functions of rigidity with total errors. For display purposes only, the F/Si and B/O flux ratios are multiplied by $\tilde{R}^{0.3}$. The solid red and blue curves show the F/Si and B/O fit results using Eq. (2), respectively. As seen, the rigidity dependence of F/Si and B/O flux ratios are distinctly different. Right panel: The 11-year AMS $\frac{F/Si}{B/O}$ ratio as a function of rigidity with total errors. The solid blue curve shows the fit results using Eq. (2). Above 10 GV, the $\frac{F/Si}{B/O}$ ratio can be described by a single power law $\propto R^\delta$ with $\delta = 0.055 \pm 0.006$ ($> 7\sigma$ difference from zero).

5. Conclusions

We have presented precision measurements of the fluxes of secondary cosmic rays Li, Be, B, and F from 2 GV to 3 TV based on the first 11 years of AMS data. Above 200 GV, the secondary cosmic rays exhibit twice as much hardening as the primary cosmic rays. The rigidity dependence of the heavier secondary-to-primary F/Si flux ratio is distinctly different from that of the lighter B/O flux ratio. In particular, above 10 GV, the $\frac{F/Si}{B/O}$ ratio can be described by a power law $\propto R^\delta$ with $\delta = 0.055 \pm 0.006$. This reveals that Li-Be-B and F belong to two different classes of secondary cosmic rays, highlighting the distinct propagation properties between heavy cosmic rays (from F to Si) and light cosmic rays (from He to O).

Acknowledgements

We acknowledge the continuous support from MIT and its School of Science. We are grateful for the support of the U.S. Department of Energy (DOE), Office of Science (DE-SC-0011848). We thank the strong support from CERN IT department.

References

- [1] Q. Yan and V. Choutko, *Eur. Phys. J. C* **83** (2023) 245.
- [2] G. Ambrosi., V. Choutko, C. Delgado, A. Oliva, Q. Yan, and Y. Li, *Nucl. Instrum. Methods Phys. Res. A* **869** (2017) 29.

- [3] Y. Jia, Q. Yan, V. Choutko, H. Liu, and A. Oliva, *Nucl. Instrum. Methods Phys. Res. A* **972** (2020) 164169.
- [4] V. Bindi et al., *Nucl. Instrum. Methods Phys. Res. A* **743** (2014) 22.
- [5] M. Aguilar et al., *Phys. Rep.* **894** (2021) 1.
- [6] M. Aguilar et al., *Phys. Rev. Lett.* **120** (2018) 021101.
- [7] M. Aguilar et al., *Phys. Rev. Lett.* **126** (2021) 081102.
- [8] Q. Yan, V. Choutko, A. Oliva, and M. Paniccia, *Nucl. Phys. A* **996** (2020) 121712.
- [9] M. Aguilar et al., *Phys. Rev. Lett.* **115** (2015) 211101.
- [10] J. Berdugo, V. Choutko, C. Delgado, and Q. Yan, *Nucl. Instrum. Methods Phys. Res. A* **869** (2017) 10.
- [11] S. Agostinelli et al., *Nucl. Instrum. Methods Phys. Res. A* **506** (2003) 250.
- [12] E. Juliusson, *Astrophys. J.* **191** (1974) 331.
- [13] R.C. Maehl, J.F. Ormes, A.J. Fisher and F.A. Hagen, *Astrophys. Space Sci.* **47** (1977) 163.
- [14] C.D. Orth, A. Buffington, G.F. Smoot and T.S. Mast, *Astrophys. J.* **226** (1978) 1147.
- [15] W. Webber and S. Yushak, in *International Cosmic Ray Conference*, vol. 12, pp. 51–56, 1979.
- [16] J. Lezniak and W. Webber, *Astrophys. J.* **223** (1978) 676.
- [17] J. Engelmann et al., *Astron. Astrophys.* **233** (1990) 96.
- [18] M. Simon et al., *Astrophys. J.* **239** (1980) 712.
- [19] S.P. Swordy et al., *Astrophys. J.* **349** (1990) 625.
- [20] A. Obermeier et al., *Astrophys. J.* **742** (2011) 14.
- [21] O. Adriani et al., *Astrophys. J.* **791** (2014) 93.
- [22] S. Thoudam and J.R. Hörandel, *Astron. Astrophys.* **567** (2014) A33.
- [23] P. Blasi, E. Amato and P.D. Serpico, *Phys. Rev. Lett.* **109** (2012) 061101.
- [24] N. Tomassetti, *Phys. Rev. D* **92** (2015) 081301.
- [25] A.E. Vladimirov, G. Johannesson, I.V. Moskalenko and T.A. Porter, *Astrophys. J.* **752** (2012) 68.
- [26] M. Aguilar et al., *Phys. Rev. Lett.* **119** (2017) 251101.
- [27] M. Aguilar et al., *Phys. Rev. Lett.* **124** (2020) 211102.
- [28] M. Aguilar et al., *Phys. Rev. Lett.* **126** (2021) 041104.
- [29] M. Aguilar et al., *Phys. Rev. Lett.* **130** (2023) 211002.